



Multiwavelength Light Curves of Two Remarkable Sagittarius A* Flares

G. G. Fazio¹, J. L. Hora¹, G. Witzel², S. P. Willner¹, M. L. N. Ashby³, F. Baganoff⁴, E. Becklin⁵, S. Carey⁶, D. Haggard⁷, C. Gammie⁸, A. Ghez⁹, M. A. Gurwell¹⁰, J. Ingalls⁶, D. Marrone¹¹, M. R. Morris¹², and H. A. Smith¹

¹ Harvard-Smithsonian Center for Astrophysics, 60 Garden Street, MS-65, Cambridge, MA 02138, USA; gfazio@cfa.harvard.edu

² University of California, Los Angeles, 475 Portola Plaza, Los Angeles, CA 90095, USA

³ Harvard-Smithsonian Center for Astrophysics, 60 Garden Street, MS-66, Cambridge, MA 02138, USA

⁴ Massachusetts Institute of Technology, 77 Massachusetts Avenue, 37-555, Cambridge, MA 02139, USA

⁵ University of California, Los Angeles, Los Angeles, CA 90095-1562, USA

⁶ California Institute of Technology, MS 314-6, Pasadena, CA 91125, USA

⁷ McGill University, 3600 University Street, Montreal, QC H3A 2T8, Canada

⁸ University of Illinois at Urbana-Champaign, 1002 West Green Street, Urbana, IL 61801, USA

⁹ University of California, Los Angeles, Los Angeles, CA 90095, USA

¹⁰ Harvard-Smithsonian Center for Astrophysics, 60 Garden Street, MS-42, Cambridge, MA 02138, USA

¹¹ University of Arizona, 933 North Cherry Avenue, Tucson, AZ 85721, USA

¹² University of California, Los Angeles, Box 951547, Los Angeles, CA 90095-1547, USA

Received 2018 March 23; revised 2018 July 9; accepted 2018 July 17; published 2018 August 30

Abstract

Sgr A*, the supermassive black hole (SMBH) at the center of our Milky Way Galaxy, is known to be a variable source of X-ray, near-infrared (NIR), and submillimeter radiation and therefore a prime candidate to study the electromagnetic radiation generated by mass accretion flow onto a black hole and/or a related jet. Disentangling the power source and emission mechanisms of this variability is a central challenge to our understanding of accretion flows around SMBHs. Simultaneous multiwavelength observations of the flux variations and their time correlations can play an important role in obtaining a better understanding of possible emission mechanisms and their origin. This paper presents observations of two flares that both apparently violate the previously established patterns in the relative timing of submillimeter/NIR/X-ray flares from Sgr A*. One of these events provides the first evidence of coeval structure between NIR and submillimeter flux increases, while the second event is the first example of the sequence of submillimeter/X-ray/NIR flux increases all occurring within ~ 1 hr. Each of these two events appears to upend assumptions that have been the basis of some analytic models of flaring in Sgr A*. However, it cannot be ruled out that these events, even though unusual, were just coincidental. These observations demonstrate that we do not fully understand the origin of the multiwavelength variability of Sgr A* and show that there is a continued and important need for long-term, coordinated, and precise multiwavelength observations of Sgr A* to characterize the full range of variability behavior.

Key words: accretion, accretion disks – black hole physics – Galaxy: center – infrared: general – submillimeter: general – X-rays: individual (Sgr A*)

Supporting material: data behind figures

1. Introduction

Sagittarius A* (Sgr A*), the supermassive black hole (SMBH) at the center of our Milky Way Galaxy, is 100 times closer than any other SMBH and is therefore a prime candidate to study the electromagnetic radiation generated by mass accretion flow onto a black hole and/or a related jet. Sgr A* has been targeted for decades in attempts to learn about SMBH physics from its variability at many wavelengths. Rapid fluctuations have been detected at soft and hard X-ray bands (Baganoff et al. 2001; Nowak et al. 2012; Neilsen et al. 2013, 2015; Barrière et al. 2014; Ponti et al. 2015) and at near-infrared (NIR) wavelengths (Genzel et al. 2003; Ghez et al. 2004; Hornstein et al. 2007; Witzel et al. 2012, 2018; Hora et al. 2014), where the extinction to the Galactic center is relatively low. Slower and lower-amplitude variability has been seen at submillimeter, millimeter, and radio wavelengths (Mauerhan et al. 2005; Macquart & Bower 2006; Yusef-Zadeh et al. 2006b; Marrone et al. 2008; Brinkerink et al. 2015). Disentangling the power source and emission mechanisms of the variability is a central challenge to our understanding of accretion flows around SMBHs at the cores of normal galaxies.

The chief barrier to progress is the absence of a sufficient sample of simultaneous, multiwavelength variability measurements, their correlations being key to discriminating among emission models (Neilsen et al. 2015; Dibi et al. 2016; Connors et al. 2017).

X-ray variability of Sgr A* has been observed by *Chandra*, *XMM-Newton*, and *Swift* at energies of 2–8 keV and by *NuStar* at 2–79 keV. X-ray flares are observed at the rate of ~ 1.1 per day and typically last ~ 0.8 hr (Neilsen et al. 2015; Ponti et al. 2015). There is often temporal substructure within X-ray flares (Baganoff et al. 2001, 2003; Goldwurm et al. 2003; Porquet et al. 2003, 2008; Eckart et al. 2004, 2006a; Belanger et al. 2005; Trap et al. 2011; Nowak et al. 2012; Degenaar et al. 2013; Neilsen et al. 2013, 2015; Barrière et al. 2014) even on timescales as short as ~ 100 s (Nowak et al. 2012; Barrière et al. 2014; Neilsen et al. 2015). The fast variability indicates that the flares come from regions smaller than ~ 10 light minutes (< 15 Schwarzschild radii). Flare amplitudes range from a few to 10 times the quiescent flux with rarer flares extending to factors of up to 400 times quiescence (Porquet et al. 2003; Dodds-Eden et al. 2011; Nowak et al. 2012; Ponti et al. 2017). The quiescent

flux ($L_{(2-10\text{ keV})} \sim 2 \times 10^{33} \text{ erg s}^{-1}$) is spatially extended ($\sim 1''$) and extremely faint (Baganoff et al. 2003; Wang et al. 2013), while the flaring source is $\leq 1''$ in size and bright.

At NIR wavelengths, as observed by VLT and Keck (1.6–3.8 μm), there is a continuously variable flux that exceeds the measurement noise level (0.033 mJy for VLT and 0.017 mJy for Keck) about 60% of the time for the VLT observations and 90% of the time for Keck observations (Witzel et al. 2012; Meyer et al. 2014). With *Spitzer*, emission at 4.5 μm was detected above the noise level $\sim 34\%$ of the time for 1 minute averaging and $>60\%$ of the time for 6.4 minute averaging (Hora et al. 2014; Witzel et al. 2018). Observed flux densities at 2.2 μm ranged from 0 to ~ 8 mJy (Witzel et al. 2018). Although the NIR light curve superficially resembles a quiescent state interrupted by brief flares, that appearance is misleading. Witzel et al. (2018) showed that the underlying probability density function of NIR flux densities is continuous and well fit by a log-normal distribution, and the time dependence is a random walk process. The apparent flares are merely the highest levels within the continuous flux-density distribution, and there is continuous variability below the typical noise level. This gives the impression of discrete outbursts, so referring to NIR peaks as “flares” is an apt description of the observed behavior at typical S/N level, but the source has no separate flaring state. Brighter flux-density levels (~ 5 –10 mJy) occur about 4–5 times per day (Witzel et al. 2012; Hora et al. 2014). These events have a duration of ~ 0.5 –2 hr with substantial temporal substructure including variations on timescales of 47 s (Dodds-Eden et al. 2009). As with X-rays, the temporal substructure implies emission from very compact regions. The NIR emission is strongly polarized, suggesting its origin is synchrotron radiation (Eckart et al. 2006b). The spectral index α ($S_\nu \propto \nu^\alpha$) measured between 1.6 and 3.7 μm during bright output intervals is 0.6 ± 0.2 (Hornstein et al. 2007), which suggests that the NIR photons are optically thin synchrotron emission from electrons with a power-law energy spectrum. The spectral index is redder during fainter intervals (Witzel et al. 2018).

At millimeter/submillimeter wavelengths, as observed by the Submillimeter Array (SMA; 875 μm and 1.3 mm), the Atacama Pathfinder Experiment telescope (870 μm), and the Caltech Submillimeter Observatory (450 and 850 μm), there is a relatively continuous emission at flux densities of ~ 3 Jy at 850 μm and 3.5 Jy at 1300 μm . This is the highest luminosity observed at any wavelength. In addition to the continuous emission, there are ~ 1.2 flaring events per day on timescales of hours to days with amplitudes $\sim 25\%$ or greater of the continuous emission (Eckart et al. 2006a; Marrone et al. 2006, 2008; Yusef-Zadeh et al. 2008). However, our observations (2004–2007) of submillimeter emission using the SMA and Atacama Large Millimeter/submillimeter Array (ALMA) produced a rate of $\sim 4.6/\text{day}$. The submillimeter continuous emission level of Sgr A* varies and, as a result, it is difficult to determine what is a flare event. Linear polarization has also been observed in submillimeter flare emission, increasing from 9% to 17% as the flare progresses through its temporal peak (Marrone et al. 2006).

Herschel/SPIRE monitored Sgr A* at far-infrared wavelengths (250, 350, and 500 μm) and observed highly significant variations with temporal structure that was highly correlated across these wavelengths, but the variability amplitude was a maximum of ~ 0.4 Jy, which is $\leq 20\%$ of the 450 μm flux

density from Sgr A* (Marrone et al. 2006; Stone et al. 2016). Recently, von Fellenberg et al. (2018), during one observation obtained with *Herschel*/PACS, measured simultaneous variation of Sgr A* at 160 and 100 μm . The observed peak emission from the median flux at 160 μm was (0.27 ± 0.07) Jy and at 100 μm was (0.16 ± 0.10) Jy.

Following the discovery of NIR and X-ray variability, coordinated observing campaigns over a range of wavelengths were initiated. The first flare of Sgr A* to be observed simultaneously at NIR and X-rays occurred in 2004 (Eckart et al. 2004). However, it has proven very difficult to obtain a sufficient number of simultaneous flares at X-ray and NIR wavelengths to determine their relationship (Eckart et al. 2006b, 2008, 2012; Yusef-Zadeh et al. 2006a, 2012; Hornstein et al. 2007; Marrone et al. 2008; Dodds-Eden et al. 2009; Ponti et al. 2017). In a total of ~ 60 hr in blocks of 3 to 7 hr of simultaneous NIR and X-ray observations using VLT/Keck and *Chandra*, there were five X-ray flares observed with corresponding NIR emission. In three of the events, peak flux occurred nearly simultaneously at both wavelengths (Figure 1). Strong X-ray flares always showed a coincident NIR maximum, but there were numerous NIR maxima with no X-ray counterpart (Eckart et al. 2004; Hornstein et al. 2007; Figure 1). Yusef-Zadeh et al. (2012) and Ponti et al. (2017) found evidence that X-ray peak emission lagged behind the NIR peak emission with a time delay ranging from a few to tens of minutes. The substructure and FWHM of coincident events differed at the two wavelengths, with the FWHM of the NIR emission wider than the X-ray emission.

Associating radio/submillimeter flares with NIR and X-ray flares has been more difficult than establishing the NIR/X-ray connection. The first observations of a flare of Sgr A* detected at submillimeter, NIR, and X-ray wavelengths were reported by Marrone et al. (2008). There are other examples of seemingly related events seen in the submillimeter near the time of NIR and/or X-ray flares (Eckart et al. 2008). However, given the multi-hour duration of typical submillimeter brightening events, the short submillimeter observing windows (nearly all less than 8 hr), and the infrequency of these events, there is some chance that the submillimeter events are only coincidentally related to the shorter-wavelength activity. Using only the Keck data (Marrone et al. 2008), an apparent delay of 20 minutes was reported between the NIR and 1.3 mm peaks. However, when the VLT NIR data were added, extending the light curve, a 160 minute delay was observed (Meyer et al. 2008). Morris et al. (2012) summarized the reported time lags between NIR and millimeter/submillimeter peaks for seven events. The delays ranged from 90 minutes to 200 minutes, with one possible exception, but on average, the delay appeared to be ~ 150 minutes.

The origin of the NIR and X-ray brightening fluctuations remains unknown, but the rapid modulation suggests the emission source most likely originates just outside the event horizon. Study of the light curves may therefore provide insight into the structure and conditions in the inner accretion regions. (See the review by Morris et al. 2012.) The near-simultaneity of the NIR and X-ray brightness fluctuations suggests a common origin, but the fact that not all NIR peaks are accompanied by X-ray flares suggests that either there are two physical origins for the NIR events or that the physical mechanism for the flares has two different observational manifestations, e.g., different flares arise from electron energy distributions having different

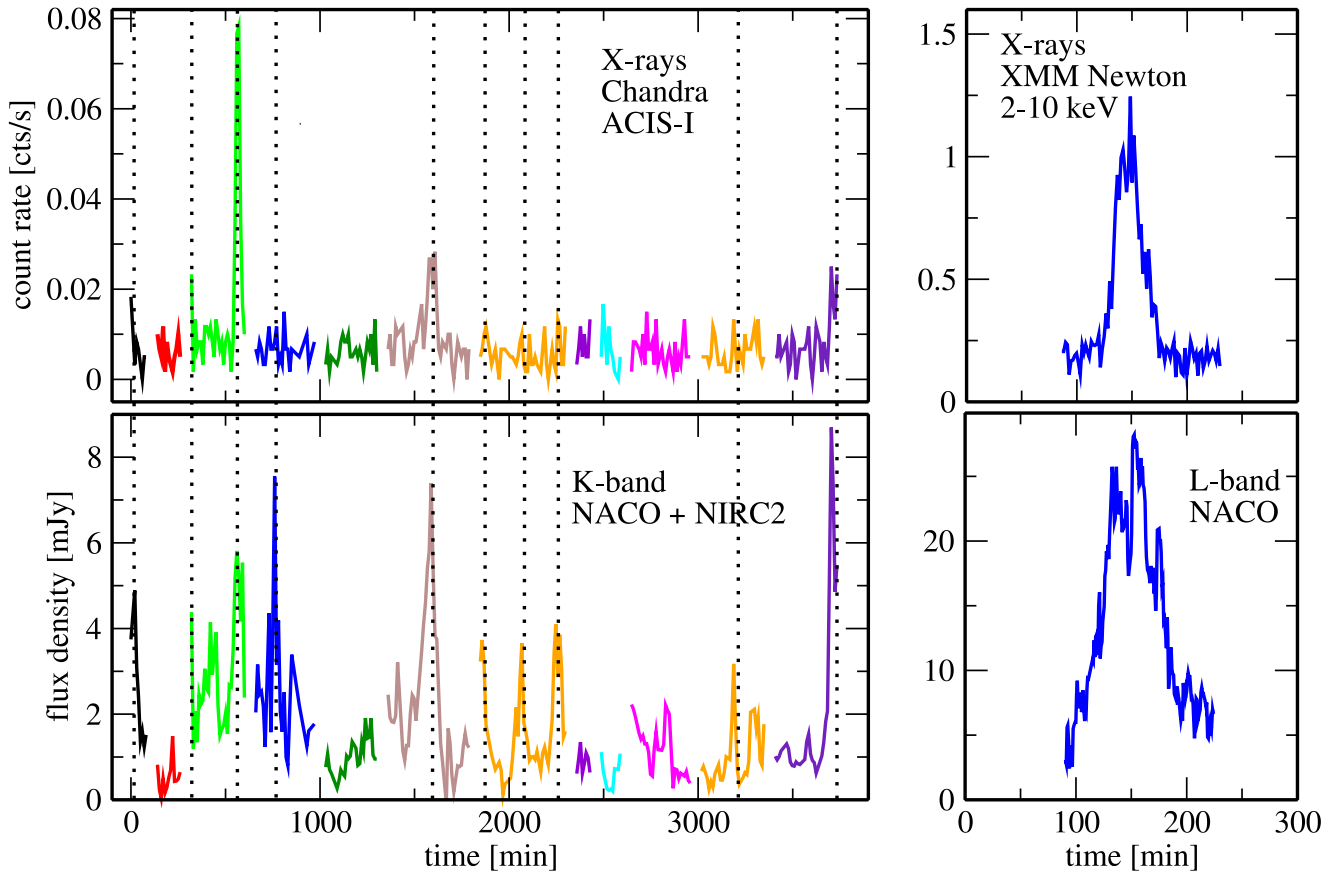


Figure 1. Left: a total of ~ 58 hr of simultaneous observations with VLT/NACO at $2.18\ \mu\text{m}$ and Keck/NIRC2 at $2.12\ \mu\text{m}$ and *Chandra X-ray Observatory*/ACIS-I at 2–8 keV is displayed. The minimum observed flux density of 3.05 mJy was subtracted from the NIR data before plotting. Observations were taken in separate 3–7 hr intervals as shown by the colors but are merged here on a continuous time axis. Vertical lines mark NIR peaks. This graph was provided by Zhiyuan Li. Right: the X-ray (2–10 keV; *XMM-Newton*) and the L-band ($3.8\ \mu\text{m}$; VLT/NACO) data from the very bright 2007 April 4 flare (Dodds-Eden et al. 2009). The data used to create this figure are available.

high-energy cutoffs, so some have enough energy to emit X-rays and some do not.

Despite the past multiwavelength monitoring over several years, Sgr A* can still surprise us. This paper presents observations of two flares that seem to violate the previous patterns in the relative timing of submillimeter/NIR/X-ray flares from Sgr A*. One of these flares provides the first evidence of near time coincidence between an NIR and submillimeter outburst, while the second event is the first example of an X-ray flare followed by a submillimeter outburst followed by an NIR peak, all within ~ 1 hr.

This paper is organized as follows. Section 2 describes the data. The flares and their properties are shown in Sections 3, and 4 offers possible interpretations for the origin of these events.

2. Observations

Two epochs of simultaneous observations of Sgr A* are reported here. The first was on 2014 June 17–18 with the *Spitzer Space Telescope*/IRAC at $4.5\ \mu\text{m}$ and the SMA at 343 GHz ($875\ \mu\text{m}$). The second was on 2015 May 14 with the Keck telescope at $2.12\ \mu\text{m}$, the SMA at 227 GHz ($1.32\ \text{mm}$), and the *Chandra X-ray Observatory* at 2–8 keV.

2.1. Spitzer/IRAC Observations

All *Spitzer*/IRAC (Fazio et al. 2004) observations used here were part of the *Spitzer* PID 10060 program (PI: G. Fazio; Hora et al. 2014), which observed Sgr A* at $4.5\ \mu\text{m}$ during four epochs of ~ 23.4 hr each. IRAC was operated in subarray mode, which obtains 64 consecutive images (a “frame set”) of a 32×32 pixel region ($1''.21$ per pixel) near the corner of the 256×256 pixel array. The observations used a subarray frame time of 0.1 s for a duration of 6.4 s for each frame set. The observing sequence after the first slew to the field included an initial mapping operation and then two successive 11.6 hr staring mode observations, each using the “PCRS Peak-up” to center Sgr A* on pixel (16,16) of the subarray. The first stare began at 2014 June 17 18:57:17 UT (HMJD 56825.7907247). The details of the data acquisition are described by Hora et al. (2014) and the data reduction by Witzel et al. (2018), who also provided the observed light curves. Because of the data reduction method, the zero point of the IRAC light curves is undetermined. Tabulated flux densities are relative to the average value when Sgr A* was in a low-emission mode.

2.2. Keck Observations

Observations amounting to 144 minutes were conducted with the adaptive optics (AO)-supported near-infrared camera

NIRC2 at the Keck II telescope of the W. M. Keck Observatory on Mauna Kea, Hawaii. We used standard observation scripts for the central $10'' \times 10''$ of our Galaxy. The same scripts have been used to track the orbital motions of stars at the Galactic center (e.g., Ghez et al. 2005, 2008; Meyer et al. 2014; Boehle et al. 2016). The observation started at 2015 May 14 12:18:10.7 UT, and the last integration ended at 14:02:01.9 UT (MJD 57156.51262–57156.58474). One hundred five frames were taken in the K band ($\lambda = 2.12 \mu\text{m}$; $\Delta\lambda = 0.35 \mu\text{m}$) in a small offset dither pattern with a cadence of ~ 15 s. For these observations the laser guide star position was fixed in the center of the image, and USNO-A2.0 0600-28577051 ($R = 13.7$) was used as tip and tilt guide star.

The observing conditions were variable, and the laser launch telescope temporarily iced over, resulting in variable FWHM values of 70–110 mas and Strehl ratios consistently below 20%. However, we were able to make use of 100 frames for photometry on Sgr A*. Following the steps described by Witzel et al. (2012), we derived for each frame a point-spread function (PSF) using the PSF-fitting package StarFinder (Diolaiti et al. 2000) and deconvolved the innermost $4'' \times 4''$ of the frame. We then used aperture photometry (circular apertures with radius of 30 mas) to determine the brightness of 13 calibrators, Sgr A*, and 6 background apertures. We used the calibrator magnitudes listed by Witzel et al. (2012), and we subtracted the measured average sky brightness. As a result we obtained a light curve for Sgr A* with an accuracy of 5%–7% in relative photometry.

2.3. The Millimeter/Submillimeter Observations

On 2014 June 18 the SMA observed Sgr A* from UT 7.4–13.5 hr (start time \sim HMJD 56826.3083) at 342.971 GHz ($875 \mu\text{m}$) with eight antennas operational in the compact configuration (baseline lengths of 14.9–99.4 k λ). The total continuum bandwidth was ~ 8 GHz. The SMA was operated in a dual-receiver polarization track with double sideband observations using sideband separation implemented in the correlator. During the observations, the precipitable water vapor (pwv) ranged from 1.2 to 1.6 mm. The continuum visibility was calculated by averaging the two same-sense polarization signals. The gain calibration source was QSO J1733–1304 (=NRAO 530), and Neptune was used as the flux calibration source. The final flux-density measurement was determined by vector-averaging the measured visibility data for instantaneous baselines greater than 40 k λ to avoid including large-scale emission structure around Sgr A*.

On 2015 May 14 the SMA again observed Sgr A* from UT 9.3 to 16.1 hr (MJD 2457156.89024) at 226.881 GHz (1.32 mm) with six antennas operational in the extended configuration (baseline lengths of 12.1–129.5 k λ). However, after UT 13.5 hr correlator issues affected the data resulting in reduced temporal coverage. The total continuum bandwidth was ~ 8 GHz. The SMA was operated in a single receiver polarization track with double sideband observations using sideband separation implemented in the correlator. At the startup of the observations the pwv was 1.8 mm, dropped within 1.5 hr to 0.9 mm, and then dropped more slowly to 0.7 mm. The continuum visibility and gain calibration were like the 2014 June 18 observations but with Calisto and Titan as the flux calibrators. The final flux-density measurement again used only baselines >40 k λ .

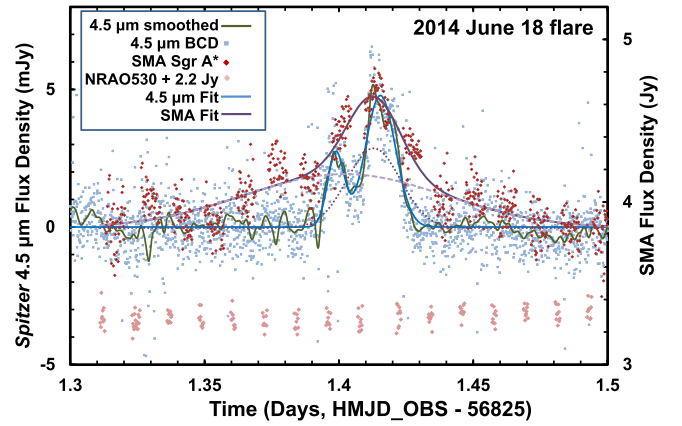


Figure 2. 2014 June 18 joint observations of a double-peaked flare from Sgr A* by *Spitzer*/IRAC at $4.5 \mu\text{m}$ (blue dots and green smoothed line, scale on the left ordinate) and the SMA at $875 \mu\text{m}$ (red dots, scale on the right ordinate). The SMA calibrator (NRAO 530) flux density (shown in light red at the bottom) is ~ 1 Jy (a constant of 2.2 Jy was added to place the data on the right ordinate scale). The blue smoothed line is the two-Gaussian curve fit to the $4.5 \mu\text{m}$ data. Dotted and dashed purple lines show two Gaussian curves fitting the SMA submillimeter data, and the solid purple line shows their sum. The data used to create this figure are available.

2.4. X-Ray Observations

Sgr A* was observed during *Chandra*'s Cycle 16 on 2015 May 14 beginning at 08:45:44 UTC (MJD 57156.36509) for a total of 22.74 ks (ObsID 16966). The data were acquired using the ACIS-S3 chip in FAINT mode with a $1/8$ subarray centered on the radio position of Sgr A*: 17:45:40.0409, $-29:00:28.118$ (J2000.0; Reid & Brunthaler 2004). The small subarray was adopted to mitigate photon pileup in bright flares from Sgr A* and to avoid contamination from nearby X-ray binaries; it has the ancillary advantage of achieving a frame time of ~ 0.4 s (versus the standard *Chandra* frame time of 3.2 s). *Chandra* data reduction and analysis were performed with standard CIAO v4.8 tools (Fruscione et al. 2006)¹ and calibration database v4.7.2. We reprocessed the level 2 events file with the *Chandra* repro script to apply up-to-date calibrations and then extracted the 2–8 keV light curve from a circular region with a radius of $1''.25$ (2.5 pixels) centered on Sgr A*. The small extraction region and energy filter help isolate Sgr A*'s flare emission and minimize contamination from diffuse X-ray background emission (e.g., Baganoff et al. 2001; Nowak et al. 2012; Neilsen et al. 2013).

3. Results

3.1. 2014 June 18 UT

We observed a significant double-peaked NIR flare on 2014 June 18 at $\sim 09:45$ UT (HMJD 56826.41209) that occurred during simultaneous observations with the SMA ($875 \mu\text{m}$). Light curves are shown in Figure 2. There was no *Chandra* coverage of this event, and *NuSTAR* observations were heavily contaminated by the transient outburst of AX J1745.6-2901, so it is not known whether the flare produced any X-ray emission. (AX J1745.6-2901 is located $2''.4$ from Sgr A* and is not a problem for *Chandra* with its $0''.5$ angular resolution.)

The NIR light curve can be fit with two Gaussian peaks separated by 23.9 minutes. The submillimeter light curve is well fit by the sum of two Gaussian functions with much

Table 1
Sgr A* Flare of 2014 June 18 UT

Telescope	Wavelength	Time (HMJD)	Amplitude above Baseline	Width (minutes) (FWHM)	Delay from Summed SMA Peak (minutes)
<i>Spitzer</i> /IRAC	4.5 μm	56826.398857	2.7 mJy	10.5	−19.6
SMA	875 μm	56826.02082	0.33 Jy	126.8	−15.0
SMA	875 μm	56826.412940	0.49 Jy	33.8	+0.7
<i>Spitzer</i> /IRAC	4.5 μm	56826.415429	4.8 mJy	19.1	+4.3

broader FWHMs than the NIR flares. The fit parameters and the delay time with respect to the summed submillimeter peak are given in Table 1. The baseline flux density of the submillimeter data is 3.84 Jy.

3.2. 2015 May 14 UT

Simultaneous observations of Sgr A* were achieved by Keck K-band (2.12 μm), *Chandra X-ray Observatory*, and the SMA (1.32 mm) on 2015 May 14 during a flare at $\sim 11:50$ UT (MJD 57156.49311258). In this unusual event, a single-peaked flare was coincident at X-ray and submillimeter wavelengths, but the NIR peak was delayed by 65.5 minutes (Figure 3). Light curves at each wavelength can be fit by a baseline plus single Gaussian, and the results are summarized in Table 2. The NIR outburst of Sgr A* reached ~ 10.4 mJy, more than half the flux density of the star S0-2. This flare is unprecedented in several aspects: the submillimeter peak precedes the X-ray peak by 27.7 minutes, and the NIR peak is delayed from the peak of the submillimeter emission by 65.5 minutes. This has never been seen in previous events. The observation time before and after the flare is very limited, and it is possible that the peaks at different wavelengths may be associated with other flares that either preceded or followed the observed flare. In particular, the Keck observations cannot rule out an NIR peak occurring before or simultaneously with the X-ray and submillimeter peaks.

4. Discussion

The relative timing of flux increases observed at X-ray, NIR, and submillimeter wavelengths from Sgr A* can be an important tool to constrain the physical processes of how plasma behaves close to the event horizon of an SMBH.

A number of simplified phenomenological models have been proposed to explain the observed time delays in Sgr A*. In one model, the emission arises from adiabatically expanding, relativistic ($\sim 0.1c$) electron clouds (plasma blobs) that emit through the synchrotron self-absorbed mechanism. The plasma blobs are initially opaque at submillimeter wavelengths, but as they expand, they become cooler and optically thin, reaching an emission maximum at progressively longer wavelengths with time (van der Laan 1966; Eckart et al. 2006a, 2006b, 2008, 2009; Marrone et al. 2006, 2008; Yusef-Zadeh et al. 2006b, 2008, 2009). The plasma blob model also predicts that the X-ray and NIR emissions should occur nearly simultaneously because they are both optically thin throughout the expansion and come from the same source, with the X-rays arising from optically thin synchrotron self-Compton (SSC), inverse Compton processes, or synchrotron emission (Markoff et al. 2001; Liu et al. 2004, 2006; Yuan et al. 2004, 2014; Eckart et al. 2006a, 2006b, 2009, 2012; Yusef-Zadeh et al. 2006a, 2008, 2012; Dodds-Eden et al. 2009). The

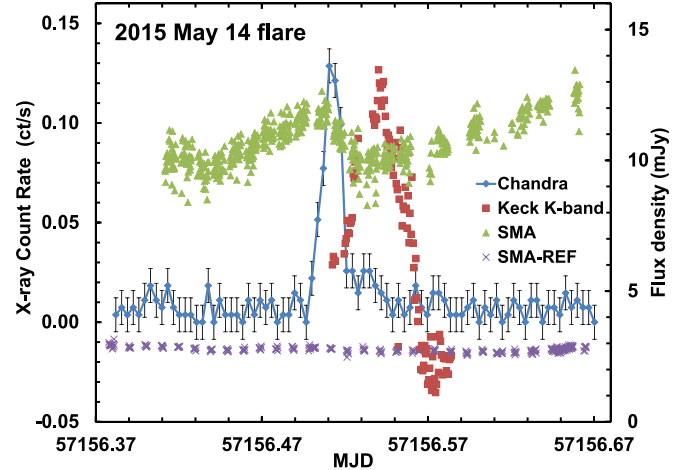


Figure 3. 2015 May 14 observations of a single-peaked flare from Sgr A*. Red squares show the Keck 2.12 μm data (scale on right ordinate), green triangles the 1.32 mm SMA data (scale is $500\times$ the right ordinate, i.e., peak flux density is ~ 6 Jy), and blue points the *Chandra* 2–8 keV data (left ordinate). The X-ray light curve is summed over 300 s bins, and Poisson error bars on the X-ray count rate are shown by black error bars. The SMA calibrator (NRAO 530) flux density (~ 1.4 Jy), scaled the same as for Sgr A*, is shown by purple crosses. The data used to create this figure are available.

SSC/expanding blob model has been used to explain the submillimeter flare time delay of ~ 150 minutes from the X-ray/NIR outburst (Yusef-Zadeh et al. 2006b, 2008, 2009; Eckart et al. 2008, 2012; Marrone et al. 2008; Wardle 2011; Morris et al. 2012; Dexter & Fragile 2013).

A jet model with shock heating of nonthermal electrons at the jet base has been proposed by Falcke & Markoff (2000) and Markoff et al. (2001); Falcke et al. (2009) have proposed a pressure-driven, mildly relativistic jet-like outflow also based on the SSC/expanding blob model. This model has been used to explain the time delay between submillimeter, millimeter, and radio outbursts, with the radio to submillimeter time lag being ~ 65 minutes between 7 and 0.86 mm wavelength (Yusef-Zadeh et al. 2006b, 2008; Bower et al. 2015; Brinkerink et al. 2015; Subroweit et al. 2017).

Other proposed models that produce some of the characteristics of the multiwavelength observations include transient orbiting hot spots, which are the product of shocks and magnetic reconnection events within the accretion flow (Broderick & Loeb 2006) and shock heating in a tilted accretion disk (Dexter & Fragile 2013). Dodds-Eden et al. (2009, 2010) and Dibi et al. (2014) have proposed a model based on a cooling break in the synchrotron radiation by nonthermal electrons in magnetized (5–30 Gauss) plasma during an accretion flow to explain X-ray and NIR simultaneous events.

Table 2
Sgr A* Flare of 2015 May 14 UT

Telescope	Wavelength or Energy	Time (MJD)	Amplitude above Baseline	Width (minutes) (FWHM)	Delay from SMA peak (minutes)
SMA	1.32 mm	57156.49311258	0.809 Jy	30.5	0
<i>Chandra</i>	4 keV	57156.51233664	0.1234 ct s ⁻¹	7.9	27.7
Keck	2.12 μ m	57156.53859682	10.36 mJy	22.1	65.5

Magnetohydrodynamic (MHD) models of accretion flow have been proposed (Goldston et al. 2005), and most recently, Moscibrodzka et al. (2014), Chan et al. (2015), and Ball et al. (2016) have created general relativistic magnetohydrodynamic (GRMHD) numerical simulation models to explain the flux increases across the electromagnetic spectrum and their relative time delays. The Chan et al. (2015) standard and normal (SANE) models reproduce the short-timescale millimeter and NIR variability with amplitudes and power spectra that are comparable to those observed. Flares in these models arise from strong-field gravitational lensing near the horizon of emission from short-lived, hot, magnetically dominated flux tubes. The SANE models also produce correlated variability only between 1.3 mm and NIR curves with small (≤ 1 hr) time lags and no correlated variability between radio, 1.3 mm, and X-ray wavelengths. This model also provides a natural explanation for the observed NIR flares with no X-ray counterpart and favors NIR emission originating in the accretion disk rather than a jet. In contrast, the Chan et al. (2015) magnetically arrested disk (MAD) models produce variability only at lower flux levels, and the radio, 1.3 mm, and NIR light curves are highly correlated, with marginal evidence of the NIR leading the 1.3 mm light curves and the radio light curves lagging the 1.3 mm by ~ 1 hr. A similar level of correlation exists between the inner X-ray and 1.3 mm light curves, with the former leading the latter by ~ 2 hr. The predicted sequence is flux increasing in the X-rays first, then the NIR, then the 1.3 mm, and then the radio flux. In the MAD models, the conjecture is that magnetic reconnection is responsible for the variability. Neither the SANE nor the MAD models produce large X-ray flares, but Ball et al. (2016) incorporated large X-ray variability by “localizing non-thermal electrons to highly magnetized regions, where particles are likely to be accelerated via magnetic reconnection. The proximity of these high-field regions to the event horizon forms a natural connection between NIR and X-ray and accounts for the rapid timescales associated with the X-ray flares.”

The 2014 June 18 flare (Figure 2), with the smoothed peaks of the NIR and submillimeter fluxes within ~ 4 minutes of each other, and the fact that the submillimeter flux rises earlier than the NIR flux, differs from previous results that the submillimeter flares follow concurrent NIR and X-ray outbursts with time delays of ~ 150 minutes. This flare sequence seems to rule out the SSC/expanding blob model and/or the jet model as its origin. The near-simultaneous NIR and submillimeter peaks may be consistent with the Chan et al. (2015) GRMHD models invoking strong lensing. Connecting the X-ray/NIR models to the submillimeter/radio models has always been difficult. However, there is the chance, for this flare, that the submillimeter event is only coincidentally related to the NIR event. The random coincidence rate (e.g., Evans 1955) for NIR/submillimeter events, assuming for the NIR 4 events day⁻¹ of

1 hr duration and for the submillimeter 1.2 events day⁻¹ of 2 hr duration, is 0.50 day⁻¹. If we assume a submillimeter event rate of 4.6 day⁻¹, then the rate is 1.9 day⁻¹. With 32 hr of NIR/submillimeter simultaneous observations from 2014 to 2017, it is possible this event is a random coincidence, even though the peak emissions of the two curves coincide within ~ 4 minutes.

For the 2014 June 18 flare, the submillimeter flux density declines from the peak by 50% in just 23 ± 5 minutes. Although each submillimeter data cluster may have a full amplitude total spread of ~ 0.4 Jy, each cluster has 30 to 40 points, and the average amplitude is therefore known with an uncertainty of ~ 0.1 Jy. The flare amplitude (peak to baseline; 4.65–3.84 Jy) is 0.81 Jy. Therefore the S/N is ~ 8 , and the peak is significant. The submillimeter calibrator has a noise level of ± 0.05 Jy. Marrone et al. (2008) observed a submillimeter decay approximated by an exponential decay time of ~ 2 hr, similar to that observed by Eckart et al. (2006b). This time is much shorter than the cooling timescale due to synchrotron losses in a ~ 20 G magnetic field. That cooling time is ~ 25 minutes in the NIR, and the cooling time for the submillimeter would be ~ 20 times slower.










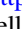



The 2015 May 14 flare (Figure 3) is unique in that the submillimeter flux density peaks first, followed ~ 28 minutes later by the X-ray peak, with the NIR peak emission occurring ~ 66 minutes after the submillimeter peak. No model we are aware of explains this sequence. However, the NIR observations began only at the peak of the X-ray flare, at which time the NIR flux was already elevated over the noise level. Because NIR events are often multi-peaked, a second, smaller NIR peak could have been associated with the X-ray flare with the subsequent, larger NIR peak being one with no X-ray association. In addition, Sgr A* is always varying at millimeter wavelengths about a mean level of ~ 3 Jy. Again, there is the chance that in the case of this flare, the X-ray, NIR, and submillimeter flux increases are only coincidentally related to each other. The random coincidence rate for X-ray/submillimeter events, assuming for the X-ray 1.1 events day⁻¹ of 1 hr duration and for the submillimeter 1.2 events day⁻¹ of 2 hr duration, is 0.14 day⁻¹. If we assume a submillimeter event rate of 3.8 day⁻¹, then the random coincidence rate is 0.4 day⁻¹.

The temporal structure of the two flare events shown in this paper implies that current theoretical models cannot explain the origin of the multiwavelength variability of Sgr A*. There is a continued and important need for long-term, coordinated, and precise multiwavelength observations of Sgr A* in order to characterize the full range of flare behaviors. The X-ray spectral index and its possible correlation with the characteristics of the NIR or submillimeter activity (peak intensity, time lags, peak duration, rise or fall times) might hold a clue to both the X-ray emission mechanism and to the underlying cause of the variability. Future coordinated monitoring should endeavor to go all the way to centimeter-wave radio in order

to determine the wavelength dependence of the phase lags, as the results in this paper show that our present view of the physical processes at work and their wavelength dependences are far from being understood. There is also a need for more detailed and more varied models of strongly sub-Eddington accretion onto SMBHs.

This work is based on observations made with the *Spitzer Space Telescope*, which is operated by the Jet Propulsion Laboratory, California Institute of Technology under a contract with NASA. We thank the staff of the *Spitzer* Science Center for their help in planning and executing these demanding observations. The W. M. Keck Observatory is operated as a scientific partnership among the California Institute of Technology, the University of California, and the National Aeronautics and Space Administration. The Observatory was made possible by the generous financial support of the W. M. Keck Foundation. The Submillimeter Array is a joint project between the Smithsonian Astrophysical Observatory and the Academia Sinica Institute of Astronomy and Astrophysics and is funded by the Smithsonian Institution and the Academia Sinica. The scientific results reported in this article are based in part on observations made by the *Chandra X-ray Observatory*. C.F.G. was supported by NSF 13-33612 and NSF 17-16327. H.S. acknowledges partial support of NASA grant NNX14AJ61G. Support for the UCLA participants for this work was provided by NSF grant AST-14-12615. Support for CfA participants was provided by NASA grant 80NSSC18K0416. We wish to thank Zhiyuan Li for providing Figure 1.

ORCID iDs

G. G. Fazio  <https://orcid.org/0000-0002-0670-0708>
 J. L. Hora  <https://orcid.org/0000-0002-5599-4650>
 G. Witzel  <https://orcid.org/0000-0003-2618-797X>
 S. P. Willner  <https://orcid.org/0000-0002-9895-5758>
 M. L. N. Ashby  <https://orcid.org/0000-0002-3993-0745>
 S. Carey  <https://orcid.org/0000-0002-0221-6871>
 D. Haggard  <https://orcid.org/0000-0001-6803-2138>
 C. Gammie  <https://orcid.org/0000-0001-7451-8935>
 A. Ghez  <https://orcid.org/0000-0003-3230-5055>
 M. A. Gurwell  <https://orcid.org/0000-0003-0685-3621>
 J. Ingalls  <https://orcid.org/0000-0003-4714-1364>
 D. Marrone  <https://orcid.org/0000-0002-2367-1080>
 M. R. Morris  <https://orcid.org/0000-0002-6753-2066>

References

- Baganoff, F. K., Bautz, M. W., Brandt, W. N., et al. 2001, *Natur*, **413**, 45
 Baganoff, F. K., Maeda, Y., Morris, M., et al. 2003, *ApJ*, **591**, 891
 Ball, D., Özel, F., Psaltis, D., & Chan, C.-k. 2016, *ApJ*, **826**, 77
 Barrière, N. M., Tomsick, J. A., Baganoff, F. K., et al. 2014, *ApJ*, **786**, 46
 Belanger, G., Goldwurm, A., Melia, F., et al. 2005, *ApJ*, **635**, 1095
 Boehle, A., Ghez, A. M., Schödel, R., et al. 2016, *ApJ*, **830**, 17
 Bower, G. C., Markoff, S., Dexter, J., et al. 2015, *ApJ*, **802**, 69
 Brinkerink, C. D., Falcke, H., Law, C. J., et al. 2015, *A&A*, **576**, 41
 Broderick, A. E., & Loeb, A. 2006, *JPhCS*, **54**, 448
 Chan, C., Psaltis, D., Özel, F., et al. 2015, *ApJ*, **812**, 103
 Connors, R. M., Markoff, S., Nowak, M. A., et al. 2017, *MNRAS*, **466**, 4121
 Degenaar, N., Miller, J. M., Kennea, J., et al. 2013, *ApJ*, **769**, 155
 Dexter, J., & Fragile, P. C. 2013, *MNRAS*, **432**, 2252
 Dibi, S., Markoff, S., Belmont, R., et al. 2014, *MNRAS*, **441**, 1005
 Dibi, S., Markoff, S., Belmont, R., et al. 2016, *MNRAS*, **461**, 552
 Diolaiti, E., Bendinelli, O., Bonaccini, D., et al. 2000, *Proc. SPIE*, **4007**, 879
 Dodds-Eden, K., Gillessen, S., Fritz, T. K., et al. 2011, *ApJ*, **728**, 37
 Dodds-Eden, K., Porquet, D., Trap, G., et al. 2009, *ApJ*, **698**, 676
 Dodds-Eden, K., Sharma, P., Quataert, E., et al. 2010, *ApJ*, **725**, 450
 Eckart, A., Baganoff, F. K., Morris, M., et al. 2004, *A&A*, **427**, 1
 Eckart, A., Baganoff, F. K., Morris, M. R., et al. 2009, *A&A*, **500**, 935
 Eckart, A., Baganoff, F. K., Schödel, R., et al. 2006a, *A&A*, **450**, 535
 Eckart, A., García-Marín, M., Vogel, N. N., et al. 2012, *A&A*, **537**, A52
 Eckart, A., Schödel, R., García-Marín, M., et al. 2008, *A&A*, **492**, 337
 Eckart, A., Schödel, R., Meyer, L., et al. 2006b, *A&A*, **455**, 1
 Evans, R. 1955, *The Atomic Nucleus* (New York: McGraw-Hill), 791
 Falcke, H., & Markoff, S. 2000, *A&A*, **362**, 113
 Falcke, H., Markoff, S., & Bower, G. C. 2009, *A&A*, **496**, 77
 Fazio, G., Hora, J. L., Allen, L. E., et al. 2004, *ApJ*, **154**, 10
 Fruscione, A., McDowell, J. C., Allen, G. E., et al. 2006, *Proc. SPIE*, **6270**, 62701
 Genzel, R., Schödel, R., Ott, T., et al. 2003, *Natur*, **425**, 934
 Ghez, A., Wright, S. A., Matthews, K., et al. 2004, *ApJL*, **601**, L159
 Ghez, A. M., Hornstein, S. D., Lu, J. R., et al. 2005, *ApJ*, **635**, 1087
 Ghez, A. M., Salim, S., Weinberg, N. N., et al. 2008, *ApJ*, **689**, 1044
 Goldston, J. E., Quataert, E., & Igumenshchev, I. V. 2005, *ApJ*, **621**, 785
 Goldwurm, A., Brion, E., Goldoni, P., et al. 2003, *ApJ*, **584**, 751
 Hora, J., Witzel, G., Ashby, M. L. N., et al. 2014, *ApJ*, **793**, 120
 Hornstein, S. D., Matthews, K., Ghez, A. M., et al. 2007, *ApJ*, **667**, 900
 Liu, S., Melia, F., Petrosian, V., & Fatuzzo, M. 2006, *ApJ*, **647**, 1099
 Liu, S., Petrosian, V., & Melia, F. 2004, *ApJL*, **611**, L101
 Macquart, J.-P., & Bower, G. C. 2006, *ApJ*, **646**, 111
 Markoff, S., Falcke, H., Yuan, F., & Biermann, P. L. 2001, *A&A*, **379**, L13
 Marrone, D. P., Baganoff, F. K., Morris, M. R., et al. 2008, *ApJ*, **682**, 373
 Marrone, D. P., Moran, J. M., Zhao, J.-H., & Rao, R. 2006, *ApJ*, **640**, 308
 Mauerhan, J. C., Morris, M., Walter, F., & Baganoff, F. K. 2005, *ApJ*, **623**, 25
 Meyer, L., Do, T., Ghez, A., et al. 2008, *ApJL*, **688**, L17
 Meyer, L., Witzel, G., Longstaff, F. A., & Ghez, A. M. 2014, *ApJ*, **791**, 24
 Morris, M. R., Meyer, L., & Ghez, A. M. 2012, *RAA*, **12**, 995
 Moscibrodzka, M., Falcke, H., Shiokawa, H., & Gammie, C. F. 2014, *A&A*, **570**, A7
 Neilsen, J., Markoff, S., Nowak, M. A., et al. 2015, *ApJ*, **799**, 199
 Neilsen, J., Nowak, M. A., Gammie, C., et al. 2013, *ApJ*, **774**, 42
 Nowak, M. A., Neilsen, J., Markoff, S. B., et al. 2012, *ApJ*, **759**, 95
 Ponti, G., De Marco, B., Morris, M. R., et al. 2015, *MNRAS*, **454**, 1525
 Ponti, G., George, E., Scaringi, S., et al. 2017, *MNRAS*, **468**, 2447
 Porquet, D., Grosso, N., Predehl, P., et al. 2008, *A&A*, **488**, 549
 Porquet, D., Predehl, P., Aschenbach, B., et al. 2003, *A&A*, **407**, L17
 Reid, M. J., & Brunthaler, A. 2004, *ApJ*, **616**, 872
 Stone, J. M., Marrone, D. P., Dowell, C. D., et al. 2016, *ApJ*, **825**, 32S
 Subroweit, M., García-Marín, M., Eckart, A., et al. 2017, *A&A*, **601**, A80
 Trap, G., Goldwurm, A., Dodds-Eden, K., et al. 2011, *A&A*, **528**, A140
 van der Laan, H. 1966, *Natur*, **211**, 1131
 von Fellenberg, S. D., Gillessen, S., Graciá-Carpio, J., et al. 2018, *ApJ*, **862**, 129
 Wang, Q. D., Nowak, M. A., Markoff, S. B., et al. 2013, *Sci*, **341**, 981
 Wardle, M. 2011, in ASP Conf. Ser. 439, *The Galactic Center: a Window to the Nuclear Environment of Disk Galaxies* (San Francisco, CA: ASP), 450
 Witzel, G., Eckart, A., Bremer, M., et al. 2012, *ApJS*, **203**, 18
 Witzel, G., Martinez, G., Hora, J., et al. 2018, *ApJ*, **863**, 15
 Yuan, F., & Narayan, R. 2014, *ARA&A*, **52**, 529
 Yuan, F., Quataert, E., & Narayan, R. 2004, *ApJ*, **606**, 894
 Yusef-Zadeh, F., Bushouse, H., Dowell, C. D., et al. 2006a, *ApJ*, **644**, 198
 Yusef-Zadeh, F., Bushouse, H., Wardle, M., et al. 2009, *ApJ*, **706**, 348
 Yusef-Zadeh, F., Roberts, D., Wardle, M., Heinke, C. O., & Bower, G. C. 2006b, *ApJ*, **650**, 189
 Yusef-Zadeh, F., Wardle, M., Dodds-Eden, K., et al. 2012, *AJ*, **144**, 1
 Yusef-Zadeh, F., Wardle, M., Heinke, C., et al. 2008, *ApJ*, **682**, 361